Hindawi Publishing Corporation
ISRN Thermodynamics
Volume 2013, Article ID 424705, 6 pages
http://dx.doi.org/10.1155/2013/424705

Research Article

Wavelength Width Dependence of Cavity Temperature Distribution in Semiconductor Diode Laser

S. P. Abbasi and A. Alimorady

Iranian National Center for Laser Science and Technology, No. 71-20th North Kargar, P.O. Box 33665-576, Tehran, Iran

Correspondence should be addressed to A. Alimorady; abolalimo@gmail.com

Received 4 July 2013; Accepted 28 August 2013

Academic Editors: J. K. Brennan and D. E. Khoshtariya

The study of heat distribution in laser diode shows that there is nonuniform temperature distribution in cavity length of laser diode. In this paper, we investigate the temperature difference in laser diode cavity length and its effect on laser bar output wavelength width that mounted on usual CS model. In this survey at the first, laser was simulated then the simulations result was compared with experimental test result. The result shows that for each emitter there is difference, about 2.5 degree between the beginning and end of cavity.

1. Introduction

High-power infrared diode laser arrays are effective sources for pumping solid-state lasers [1–3]. These laser arrays are composed of one or more laser bars; each laser bar consists of numerous individual laser emitters formed on a single piece of semiconductor [4, 5]. Various characteristics like quantum efficiency, output power, and their dependence on cavity length and composition have been discussed. There are a number of factors that limit the output power and reliability of diode lasers, for example, catastrophic optical damage and overheating. Cavity length increase was used for increasing output power [4].

In this paper at first four laser diode heat sources were considered and this distribution in the cavity was studied and was simulated. Then the temperature distribution was simulated in the single emitter in the laser diode bar that packaged on the CS mount model and then measured the temperature difference in laser diode points in cavity length. Temperature distribution effect on the wavelength width and the wavelength peak shift and other hand simulation results were compared with experimental results.

2. Laser Diode Structure and Simulation

Our simulation is based on GaAs, 20 W, CW modes, 808 μm CS laser diode. The laser diode has 19 emitters with 100 μm width stripe and 20% fill factor that was produced in INLC (Figure 1). The laser operation specification is listed in Table 1.

The mounting of laser bar on the package and the heat removing direction was shown in Figure 2 and layer structure specification is listed in Table 2 and its arrangement was shown in Figure 3. The bar dimensions, thickness, bar width (cavity length), bar length, are 117, 1000, and 9800 μm, respectively.

Laser diode thermal structure simulated in COMSOL 3.5 Multiphysics software. Geometric symmetry in laser bar can help for simplifying the geometry and then single emitter was simulated. The 150313 triangular meshes were used in this simulation for laser diode, Indium paste, and Cu heat sink body (Figure 4).

The laser was simulated in the temperature condition 27°C, current operation 25 A, and optical output power 20 W. The heat value that must be removed from laser bar equals 24.5 W.

3. Thermal Model

Temperature 3D profiles are found in the laser structure using the thermal conduction equation:

$$\begin{aligned}&\operatorname{div}\left\{k\left[T\left(x,y,z\right),x,y,z\right]\cdot\operatorname{grad}\left[T\left(x,y,z\right)\right]\right\}\\&\quad=-g_T\left[T\left(x,y,z\right),x,y,z\right],\end{aligned}\tag{1}$$

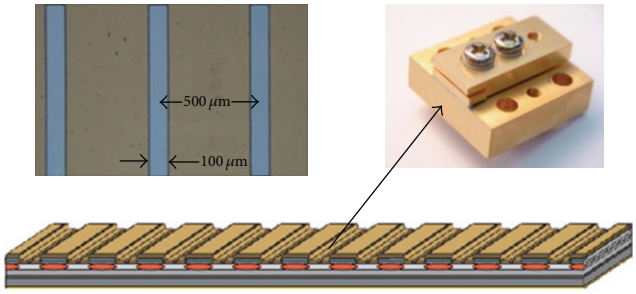

Figure 1: Schematic of laser bar, bar stripe geometry dimension, and CS model packaging laser diode.

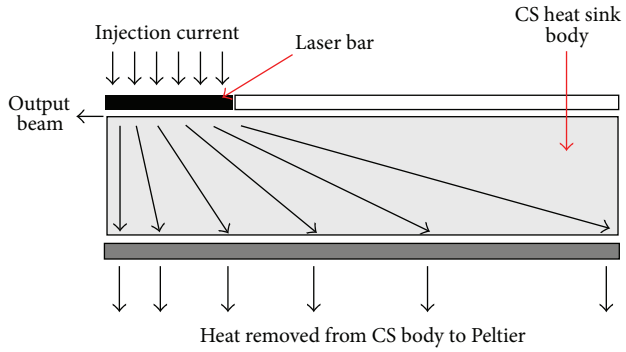

Figure 2: Bar packaging position on CS heat sink and heat removed path from the bar to TEC.

Table 1: Laser operation Characteristics.

	Parameters	Value	Unit
1	Output power	20	W
2	Threshold current	0.25	A
3	Operation current	25	A
4	Operation voltage	1.8	V
5	Serial resistance	0.007	Ω
6	Wave length peak	808 ± 3	nm

where the temperature- and position-dependent thermal conductivity k, g_T stand for the 3D distribution of heat generation (in Wm^{-3}). Heat sink is the copper ($5 \times 5\,\mathrm{mm}^2$) radiator that is properly taken into account assuming its much larger dimensions than those of the laser chip, so its external walls are assumed to remain at room temperature of the ambient. Top and sidewalls of the laser crystal are assumed to be thermally isolated because of negligible effect of thermal radiation and thermal diffusion of air particles [1].

In this simulation four heat sources were considered:

(1) nonradiative recombination,

(2) reabsorption of radiation,

(3) Joule heating,

(4) mirror absorption.

The produced heat of mirrors absorption is very smaller than the other heat sources but its effect was observed in the results.

The reflectivity of back mirror is 96–98% and for front mirror 7–10% was considered. Nonradiative recombination is proportional to the $1-\eta_i$ that η_i is internal quantum efficiency and relates the waveguide material and doping level (carriers) [4–7]. Reabsorption of radiation occurs in resonator and this process is spatially homogeneous. Diode lasers Joule heating distribution depends on spreading of injection current [4].

Current spreading and the nonuniformity effect of the injection have been studied and simulated in COMSOL 3.5 Multiphysics software in steady state analysis. The electrical model is composed of the Laplace equation:

$$\mathrm{div}\left\{\sigma\left(x,y,z\right)\mathrm{grad}\left[V\left(x,y,z\right)\right]\right\}=0. \quad (2)$$

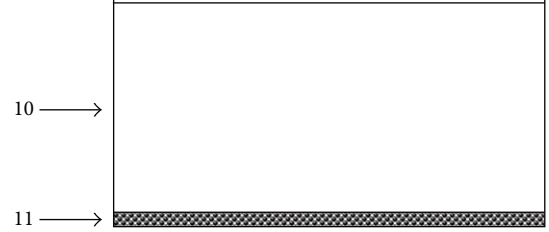

Figure 3: Laser bar structure and epitaxial layer arrangement.

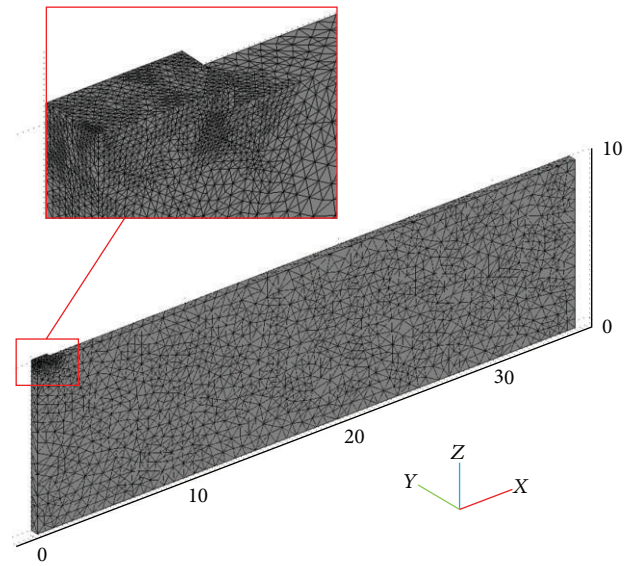

Figure 4: Laser diode and heat sink meshing in COMSOL software.

Table 2: Laser bar structure layers specification.

Number	Layers	Function	Thickness (A)	Doping (cm^{-3})
1	P contact Au/Ti/Pt	Contact	3000	—
2	SiO_2	Dielectric	1300	—
3	p-GaAs	Contacting	2500	$(3–15) \times 10^{18}$
4	p-$Al_{0.15}Ga_{0.35}In_{0.5}P$	Cladding	12000	2×10^{18}
5	$Ga_{0.17}In_{0.83}P$	SCH	4500	5×10^{17}
6	$GaAs_{0.81}P_{0.19}$	QW	160	
7	$Ga_{0.17}In_{0.83}P$	SCH	4500	5×10^{17}
8	n-$Al_{0.15}Ga_{0.35}In_{0.5}P$	Cladding	12000	2×10^{18}
9	n-GaInP	Buffer	4000	2×10^{18}
10	n-GaAs	Substrate	110000	2.2×10^{18}
11	N contact Au/Ge/Ni	Contact	4000	—

Table 3: Thermal conductivity, electrical resistivity, and electron mobility of material (300 K).

Metals and oxide materials	Thermal conductivity (W/mK)	Electrical resistivity (Ωcm)
Cu	398	1.7×10^{-6}
In	87	8.4×10^{-6}
SiO_2	1.38	10^{18}
Au	318	2.27×10^{-6}
Pt	73	108×10^{-6}
Ti	22	39×10^{-6}
Ni	92	7.2×10^{-6}
GeAu	150	6.5×10^{-3}
Semiconductor materials	Thermal conductivity (W/mK)	Mobility ($cm^2\ V^{-1}\ s^{-1}$)
GaAs	44	8500
$Al_{0.15}Ga_{0.35}In_{0.5}P$	114	2700
$Ga_{0.17}In_{0.83}P$	73	5500
$GaAs_{0.81}P_{0.19}$	61	7850

And the diffusion equation within the active region

$$D(T)\frac{d^2 n_A(y)}{dy^2} - \left[An_A(y) + B(n_A, T)n_A^2(y) + Cn_A^3(y)\right] + \frac{j_{\text{pn}}(y)}{ed_A} = 0. \tag{3}$$

In the above equations, σ stands for the 3D electrical conductivity profile, V is the 3D potential distribution, D is the temperature-dependent ambipolar diffusion constant, n_A is the active-region carrier-concentration distribution, A, B, and C are the monomolecular, the bimolecular (mostly radiative), and the Auger, respectively, recombination coefficients, $j_{\text{pn}}(y)$ stands for the p-n junction current-density distribution, e is the electron charge, and d_A is the cumulative active-region thickness. The Laplace equation, instead of the Poisson one, is used because noncompensated electric charges are confined only to the active-region area, which is treated separately [4]. Current-density profiles are calculated from the potential distribution using the Ohm's law:

$$j(x, y, z) = \sigma(x, y, z)\,\text{grad}\left[V(x, y, z)\right]. \tag{4}$$

The room temperature electrical resistivity of material and layer that was used in simulation was listed in Table 3 [1, 8, 9].

Results show that increasing the current density cannot change the Joule heating distribution in the laser diode and the main part of Joule heating is related to stripe position and only less than 6% in outside of stripe part. Figure 5 shows the current spread in laser diode in a different current.

For simulating the Joule heating, COMSOL 3.5 Multiphysic software was used in steady state analysis in the electrothermal interaction.

For ternary GaInP and GaAsP compounds and the quaternary AlGaInP at the values of the room temperature, thermal conductivities are found in [4, 8] and their relative temperature dependencies are giving finally in ($Wm^{-1}K^{-1}$):

$$k_{\text{In}_x\text{Ga}_{1-x}\text{P}} = \frac{100}{1.30 + 20.07x - 19.9x^2},$$
$$k_{\text{GaAs}_x\text{P}_{1-x}} = \frac{100}{1.30 + 22.57x - 21.6x^2}, \tag{5}$$
$$k_{\text{Al}_x\text{Ga}_y\text{In}_{1-x-y}\text{P}} = 147 - 57x - 70y.$$

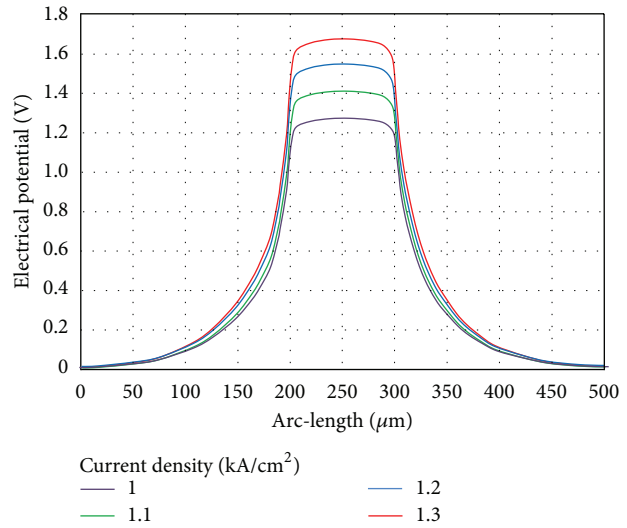

FIGURE 5: The current spread in laser diode in different currents. Stripe width and chip width are 100 μm and 500 μm, respectively.

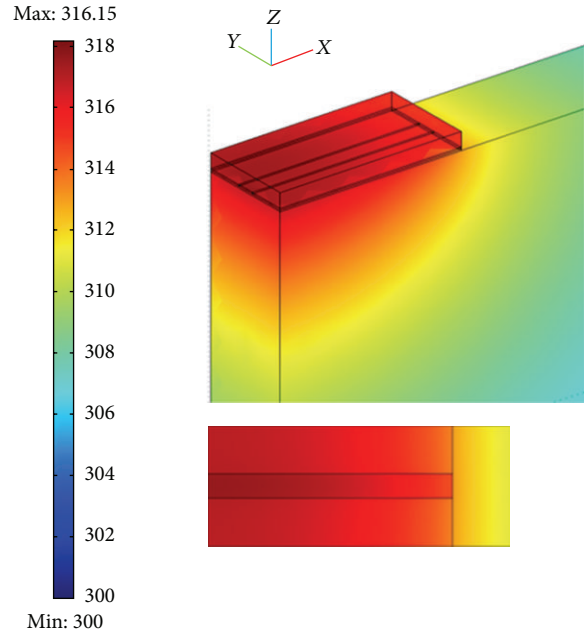

FIGURE 6: Temperature profile.

The values of the room temperature thermal conductivities relative temperature dependencies are giving finally in ($\mathrm{Wm^{-1}K^{-1}}$):

$$k_{\mathrm{GaAs}} = 44\left(\frac{T}{300}\right)^{-1.25},$$
$$k_{\mathrm{GaP}} = 77\left(\frac{T}{300}\right)^{-1.36}, \quad (6)$$
$$k_{\mathrm{InP}} = \frac{100}{[1.47 + (t - 300)/111]}.$$

To the best of the authors' knowledge, there are no published measurements of thermal conductivities relative temperature dependencies in Quaternary AlGaInP compounds. Effective thermal conductivity of a two-layer contact is calculated using the relation

$$k_{AB} = \frac{k_A k_B (d_A + d_B)}{d_A k_B + d_B k_A}, \quad (7)$$

where k_A, k_B and d_A, d_B are the thermal conductivities and the thicknesses, respectively, of both A and B layers. For a three-layer contact, this approach should be repeated [2]. The values of thermal conductivities of contact materials that were used were shown in Table 3.

Thermal conductivity of material at room temperature used in simulation was listed in Table 3. This conductivity calculated from the related equations [1].

4. Simulation Results

Figure 6 shows the temperature profile of emitter and heat sink. Figure 6 shows the top view temperature profile of the chip and the temperature difference of regions in the cavity length. There is a temperature difference between 2 regions along the cavity near the front and back mirrors. The reason

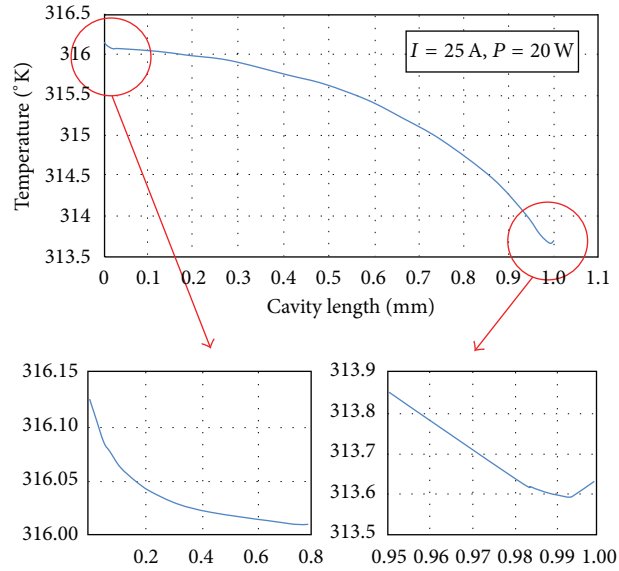

FIGURE 7: The temperature difference in cavity length and mirror effect.

of this difference is for nonsymmetric position on the heat sink in the straight line of cavity (Figure 2).

The temperature difference measuring in the cavity length was shown in Figure 7.

There are nonlinear differences near mirrors because of mirror absorption and on other hand the mirror material Al_2O_3 thermal conduction that is less than cavity material GaAs thermal conduction.

The temperature difference in cavity length in different operation currents was shown in Figure 8. The result shows

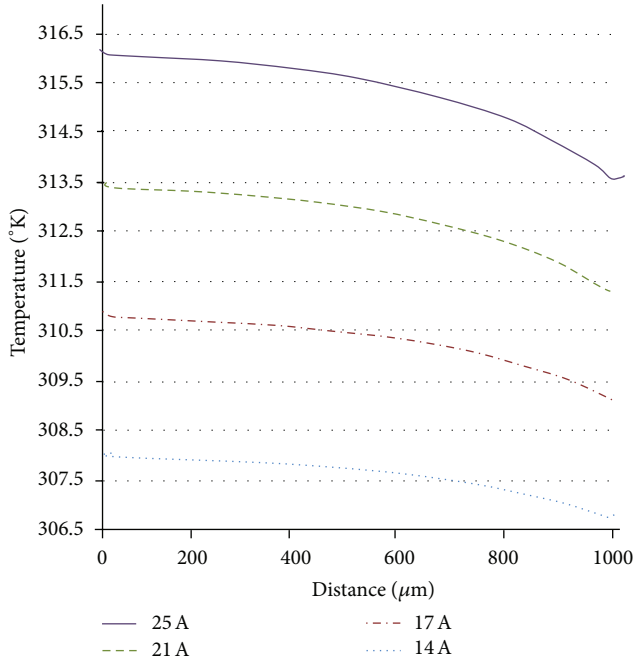

Figure 8: The temperature difference in cavity length in different operation currents.

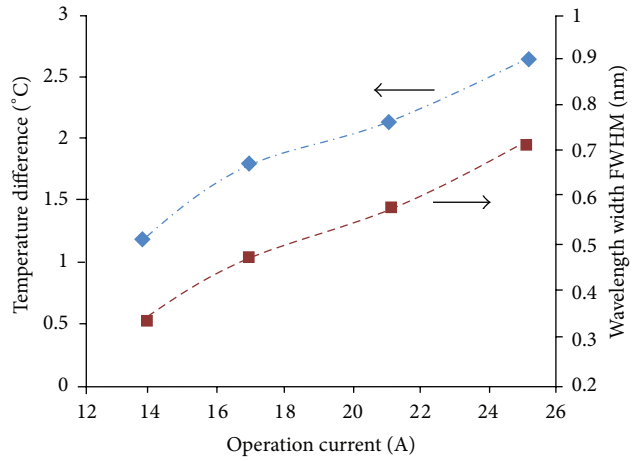

Figure 9: The wavelength width increasing in different operation currents affected by temperature difference in cavity length.

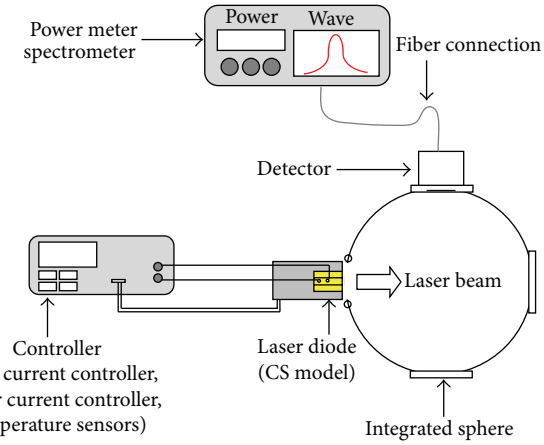

Figure 10: Experimental arrangement.

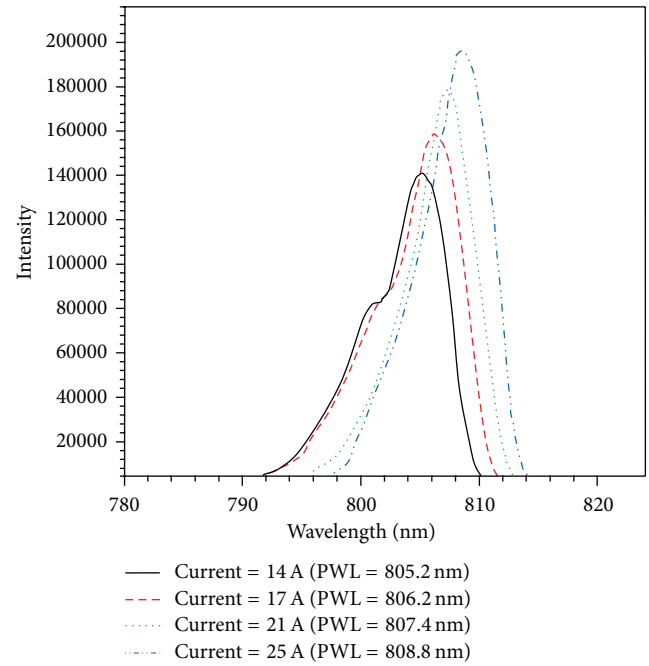

Figure 11: The experimental spectra in different operation currents.

the linear increase in this difference with increase of the operation current (Figure 8).

Simulation results for temperature difference in the cavity and the wavelength width variation for this temperature difference was shown in Figure 9. The wavelength shift value in single the cavity in simulation is 0.28 μm/°C that has agreement with experimental results which show that this value is 0.26 μm/°C.

5. Experimental Results

The experiment was arranged according to Figure 10 and the peak wavelength shift and wavelength width were measured in laser diode in different operation currents. The suitable accurate drivers and sensors control the laser current for stable power and TEC (Peltier) current for heat removing.

The spectral result was shown in Figure 11. There are differences in spectral wavelength width that was shown in Figure 12. The peak wavelength shift value is 0.26 μm/°C.

6. Result and Conclusion

Laser diode peak wavelength was shifted by temperature increase. Our survey about the heat distribution in laser diode shows that there is nonuniform temperature distribution in cavity length of laser diode. This temperature difference increases the spectral wavelength width.

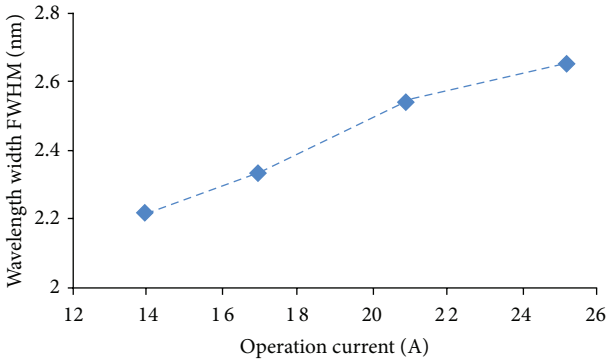

FIGURE 12: The experimental wavelength width increasing in different operation currents.

In this investigation the laser diode CS model was simulated. The result shows that there is 2.5°C difference along cavity length. This difference was increased by increasing operation current. For example, when the operation current was increased from 14 A to 25 A the temperature difference along cavity length was increased from 1°C to 2.7°C; this process increases the wavelength width from 2.2 μm to 2.7 μm. This result was confirmed with experimental results.

References

[1] B. Laikhtman, A. Gourevitch, D. Donetsky, D. Westerfeld, and G. Belenky, "Current spread and overheating of high power laser bars," *Journal of Applied Physics*, vol. 95, no. 8, pp. 3880–3889, 2004.

[2] A. Tomczyk, R. P. Sarzała, T. Czyszanowski, M. Wasiak, and W. Nakwaski, "Fully self-consistent three-dimensional model of edge-emitting nitride diode lasers," *Opto-Electronics Review*, vol. 11, no. 1, pp. 65–75, 2003.

[3] A. Gourevitch, B. Laikhtman, D. Westerfeld et al., "Transient thermal analysis of InGaAsP-InP high-power diode laser arrays with different fill factors," *Journal of Applied Physics*, vol. 97, no. 8, Article ID 084503, 6 pages, 2005.

[4] B. Mroziewicz, M. Bugajski, and W. Nakwaski, *Physics of Semiconductor Lasers*, North-Holland Science Publishers, 1991.

[5] F. Bachmann, P. Loosen, and R. Poprawe, *High Power Diode Lasers Technology and Applications*, Springer, New York, NY, USA, 2007.

[6] D. S. Patil, *Semiconductor Laser Diode Technology and Applications*, InTech, Rijeka, Croatia, 2012.

[7] S. Adachi, *Properties of Semiconductor Alloys: Group-IV, III–V and II–VI Semiconductors*, John Wiley & Sons, New York, NY, USA, 2009.

[8] A. Yariv and P. Yeh, *Photonics Optical Electronics in Modern Communications*, Oxford University Press, New York, NY, USA, 2007.

[9] D. R. Lide, *Handbook of Chemistry and Physics*, CRC Press, New York, NY, USA, 2004.